

Interplay between activator–inhibitor coupling and cell–matrix adhesion in a cellular automaton model for chondrogenic patterning

Maria A. Kiskowski,^a Mark S. Alber,^{a,*} Gilberto L. Thomas,^{b,1} James A. Glazier,^c
Natalie B. Bronstein,^{d,2} Jiayu Pu,^d and Stuart A. Newman^{d,*}

^aDepartment of Mathematics and Center for the Study of Biocomplexity, University of Notre Dame, Notre Dame, IN 46556-5670, USA

^bDepartment of Physics, University of Notre Dame, Notre Dame, IN 46556-5670, USA

^cDepartment of Physics and Biocomplexity Institute, Indiana University, Bloomington, IN 47405-710, USA

^dDepartment of Cell Biology and Anatomy, New York Medical College, Valhalla, NY 10595, USA

Received for publication 2 July 2003, revised 18 March 2004, accepted 25 March 2004

Available online 24 May 2004

Abstract

We present a stochastic cellular automaton model for the behavior of limb bud precartilaginous mesenchymal cells undergoing chondrogenic patterning. This “agent-oriented” model represents cells by points on a lattice that obey rules motivated by experimental findings. The “cells” follow these rules as autonomous agents, interacting with other cells and with the microenvironments cell activities produce. The rules include random cell motion, production and lateral deposition of a substrate adhesion molecule (SAM, corresponding to fibronectin), production and release of a diffusible growth factor (“activator,” corresponding to TGF- β) that stimulates production of the SAM, and another diffusible factor (“inhibitor”) that suppresses the activity of the activator. We implemented the cellular automaton on a two-dimensional (2D) square lattice to emulate the quasi-2D micromass culture extensively used to study patterning in avian limb bud precartilaginous cells. We identified parameters that produce nodular patterns that resemble, in size and distribution, cell condensations in leg-cell cultures, thus establishing a correspondence between *in vitro* and *in silico* results. We then studied the *in vitro* and *in silico* micromass cultures experimentally. We altered the standard *in vitro* micromass culture by diluting the initial cell density, transiently exposing it to exogenous activator, suppressing the inhibitor, and constitutively activating fibronectin production. We altered the standard *in silico* micromass culture in each case by changing the corresponding parameter. *In vitro* and *in silico* experiments agreed well. We also used the model to test hypotheses for differences in the *in vitro* patterns of cells derived from chick embryo forelimb and hindlimb. We discuss the applicability of this model to limb development *in vivo* and to other organ development.

© 2004 Elsevier Inc. All rights reserved.

Keywords: Precartilaginous condensation; Computational biology; Pattern formation; Agent-based model; Biological lattice gas model

Introduction

Skeletal pattern formation in the developing vertebrate limb depends on interactions of precartilaginous mesenchymal cells with factors that control the spatiotemporal differentiation of cartilage. A full characterization *in vivo* would require knowledge of, among other things, the roles of Hox and Tbx genes, which help distinguish between skeletal elements and limb types, and of Wnt genes, which help distinguish dorsal from ventral surfaces of the limb (reviewed in Tickle, 2003). However, the most basic skeletogenic processes involve the spatial

* Corresponding authors. Mark S. Alber, Department of Mathematics and Center for the Study of Biocomplexity, University of Notre Dame, Notre Dame, IN 46556-5670; Stuart A. Newman, Department of Cell Biology and Anatomy, New York Medical College, Basic Sciences Building, Valhalla, NY 10595.

E-mail addresses: malber@nd.edu (M.S. Alber), newman@nyc.edu (S.A. Newman).

¹ Permanent address: Instituto de Física, Universidade Federal do Rio Grande do Sul, Porto Alegre, RS 91501-970, Brazil.

² Present address: Division of Natural Sciences, Mercy College, Dobbs Ferry, NY 10522.

separation of precartilaginous mesenchyme into chondrogenic and nonchondrogenic domains.

In vitro as well as in vivo (see reviews by Hall and Miyake, 2000 and Newman and Tomasek, 1996), TGF- β s and other members of this superfamily induce precartilaginous condensation by a process that involves the upregulation of fibronectin (Leonard et al., 1991). Mesenchymal cells accumulate in regions of increased cell-matrix adhesive interactions (Downie and Newman, 1994, 1995; Frenz et al., 1989a,b) and then acquire epithelioid properties by upregulation of cell-cell adhesion molecules such as N-CAM (Widelitz et al., 1993) and N-cadherin (Delise and Tuan, 2002; Oberlender and Tuan, 1994), the expression of which is also controlled by TGF- β (Tsonis et al., 1994). Cartilage differentiation or chondrogenesis follows at the sites of condensation in vitro and in vivo.

We have suggested (Newman, 1996; Newman and Frisch, 1979) that interactions between diffusible activators and inhibitors of chondrogenesis can explain the approximately periodic patterns of chondrogenesis in the developing limb and in micromass cultures. Results of Miura and Shiota (2000a,b) and Miura et al. (2000) provide strong evidence for such a “reaction-diffusion” mechanism in vitro. In particular, TGF- β 2 acts as an activator by positively regulating its own production, as well as precartilaginous condensation (Miura et al., 2000). Mofteh et al. (2002) recently found that activation of fibroblast growth factor receptor 2 (FGFR2), which appears on cells at sites of incipient condensation, suppresses condensation in surrounding mesenchyme by eliciting production of an inhibitor of chondrogenesis. While the molecular identity of the inhibitor is unknown, it acts laterally, spreading by an unknown mechanism from its sites of production (Mofteh et al., 2002).

The formation of mesenchymal condensations in micromass cultures prepared from chicken or mouse limb precartilaginous cells provides an easily manipulated in vitro model for exploring interactions between genetic and physical processes (Delise and Tuan, 2002; Frenz et al., 1989a,b; Leonard et al., 1991; Miura and Shiota, 2000a,b; Miura et al., 2000; Mofteh et al., 2002; Newman, 1977). At the cellular level, these cultures proceed through essentially the same steps as the limb mesoblast in vivo (Hall and Miyake, 1995, 2000; Newman and Tomasek, 1996), giving rise to spatial patterns of condensation. The condensation patterns then develop into patterns of cartilage nodules with characteristic features, depending, for example, on whether the cells come from the forelimb or hindlimb (Downie and Newman, 1994, 1995). Although the patterns that form in vitro differ in important respects from those of the developing limb bud in vivo, they form over similar spatiotemporal scales, using many of the same molecular components, raising the possibility that the two processes have common underlying bases (Newman, 1996). Significantly, “recombinant” limb buds consisting of dissociated, randomized limb mesenchyme cells packed into ectoderm (Ros et al., 1994; Zwilling, 1964) can form recognizable, well-spaced

cartilage elements, suggesting that important aspects of limb skeletal pattern formation are self-organizing and would therefore also function in vitro.

Although the in vivo and in vitro systems differ in the number of cell types present and complexity of tissue organization, the distribution of Hox gene products and other regulatory molecules (reviewed in Tickle, 2003), and in overall geometry, their common features are likely to provide insight into the self-organizational aspects of skeletogenesis. Activators (such as TGF- β s: Chimal-Monroy et al., 2003; Leonard et al., 1991; Merino et al., 1998; Miura and Shiota, 2000a) and inhibitors (induced by ectodermal FGFs: Hurle et al., 1989; Mofteh et al., 2002) of chondrogenesis and associated adhesion molecules operate in both settings and constitute dynamical systems with the potential to form the requisite patterns (Newman, 1988, 1996).

Computational models can keep track of vast numbers of molecular interactions and cell behavioral changes and are therefore ideal for representing the dynamics of cellular pattern formation. Such models, if they reflect the authentic features of development, can potentially account for complex behaviors under normal conditions and predict the effects of experimental manipulations and genetic alterations.

Cellular automata (CA), one class of computational model, are dynamical systems defined on a regular lattice. While CA, unlike most biological systems, are discrete in space, time, and state, under appropriate assumptions they can model biological phenomena as varied as predator-prey dynamics in fish populations (Dewdney, 1987; Ermentrout and Edelstein-Keshet, 1993), bacterial colony growth (Kreft et al., 2001), and pacemaker activity in cardiac tissue (Kaplan et al., 1988; Winfree et al., 1985). The range of applicability and the power of such models lie in their surprisingly rich array of complex behaviors and spatial patterns, which arise from the interaction of components that follow simple rules (Wolfram, 1983, 1994a,b, 2002).

This paper presents a stochastic CA model for the formation of patterns of mesenchymal condensations in micromass cultures. As indicated above, this in vitro system provides a simplified, experimentally tractable model for skeletal patterning in the vertebrate limb. Its quasi-2D geometry suits computational modeling particularly well. Because introduction of exogenous growth factors (Leonard et al., 1991; Miura and Shiota, 2000a; Mofteh et al., 2002), alteration of gene expression (reviewed in Delise et al., 2000), and evaluation of patterns (Miura and Shiota, 2000a; Miura et al., 2000) are straightforward in the limb micromass culture, we can examine whether our computational model can represent normal and experimentally manipulated developmental pattern formation.

For the computational model to be manageable, we must select key processes from the hundreds of cell-cell and cell-gene product interactions in the limb. Our choice for the “core” patterning interactions comes from experiment and constitutes a set of hypotheses—a dynamical developmental model—for chondrogenesis in limb bud mesen-

chyme. The computational model implements and tests the developmental model.

In this study, we have defined a range of parameter values for the computational model that reproduces the size and distribution of precartilaginous condensations in micromass cultures prepared from chicken leg precartilaginous mesenchyme cells. We have then explored this “standard” model computationally with regard to roles of random cell movement, secreted substrate adhesion molecules (SAMs; e.g., fibronectin) and lateral inhibitor of condensation, effects of cell dilution and forced overexpression of substrate adhesion molecule, addition of exogenous activator (i.e., TGF- β), and differences between patterns in cultures prepared from leg and wing precartilaginous cells. In each case, the computational results are compared with experimental results, and there is good agreement.

In the following section, we describe the key features of the in vitro, developmental, and computational models.

Materials and methods

In vitro model

Our cell culture experiments use mesenchymal tissue isolated from the distal 0.3 mm of Hamburger and Hamilton (1951) stage 24–25 leg or wing buds of 5-day White Leghorn embryos (Avian Services, Inc., Frenchtown, NJ) (Downie and Newman, 1994, 1995; Frenz et al., 1989a,b). This tissue is free of myoblasts and myogenic precursors, which have not yet migrated into the limb tip at these stages (Brand et al., 1985; Newman et al., 1981); the cultures therefore consist almost entirely of precartilaginous cells. We plate the cells at 1.75×10^5 (or 1.5×10^5 for dilution experiments) per 10- μ l spot on Costar 24-well plates (Cat. No. 3526) at approximately uniform cell density in serum-free defined medium (DM; Paulsen and Solorsh, 1988). Where indicated, we added TGF- β 2 (2 ng/ml in DM) to the cultures 24 h after plating and washed it out with DM 5 h later (Leonard et al., 1991). Downie and Newman (1994) provide additional culture details. Imaging of living cultures used Hoffman Modulation Contrast microscopy (Modulation Optics, Inc., Greenvale, NY), with condenser and polarizer adjusted to visualize cell condensations (Frenz et al., 1989b). We fixed some cultures of each group after 6 days of incubation and stained for cartilage matrix with Alcian blue at pH 1.0 (Downie and Newman, 1994).

Transfection

Stage 24 leg bud tips were suspended in 1 ml phosphate-buffered saline (0.02 M sodium phosphate buffer, 0.15 M NaCl, pH 7.4) containing 10 μ g capped mRNA synthesized using the messageMachine kit (Ambion) with a template consisting of a 843 b cDNA sequence encoding the 29-kDa amino-terminal heparin-binding domain of chicken fibro-

nectin preceded by the natural fibronectin secretory signal sequence (Pu, 1999) cloned into pBluescript (Stratagene). We applied three 50-ms 2-V pulses to the tissue in a BTX Electro Square Porator T820 equipped with an Enhancer 400 oscilloscope (Genetronics, Inc., San Diego, CA) in a 4-mm gap BTX electroporation cuvette (Moftah et al., 2002). The limb tips were then treated with trypsin, dissociated, and plated as described above.

Developmental model

Our basic developmental model for precartilaginous condensation consists of the following elements:

- (i) Limb mesenchymal cells move randomly with a constant diffusion rate unless their extracellular matrix or surface adhesive properties change.
- (ii) All cells can produce TGF- β .
- (iii) TGF- β stimulates cells to produce more TGF- β .
- (iv) Cells in incipient condensations secrete a lateral inhibitor of condensation.
- (v) TGF- β induces cells to produce fibronectin and N-cadherin.
- (vi) Cell motility decreases in matrices containing elevated levels of fibronectin.
- (vii) N-cadherin promotes cell–cell adhesion.

All these elements of the developmental model have experimental support, as noted above. Fig. 1 presents a schematic diagram of the gene product interactions that the computational model employs.

Computational model

Our computational model contains three components.

First, we model cells as occupied nodes of a square lattice (i.e., a rectangular grid) whose default behavior is

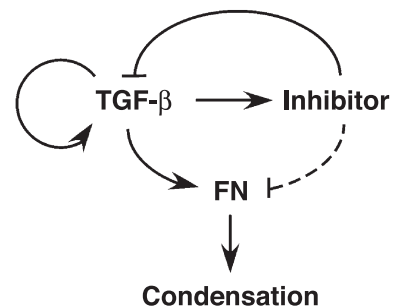


Fig. 1. Gene product interactions leading to limb precartilaginous mesenchymal condensation. This schematic diagram summarizes the major features of the developmental system the computational model simulates. The text discusses the experimental bases of the various steps. The molecular identity of the lateral inhibitor of condensation (Moftah et al., 2002) is unknown. This inhibitor may act at the level of TGF- β synthesis or activity (solid inhibitory vector), fibronectin synthesis (dashed inhibitory vector), or at some earlier stage. For the purposes of our computational model, we assume it acts on the activator (i.e., TGF- β).

random walk diffusion (analogous to Brownian motion). We assume all cells are identical.

Second, we simulate on the lattice a cell-driven process that depends on the interaction between two molecular species: a diffusible activator, A, which we identify with TGF- β in the developmental model, and an inhibitor, B, which we identify with the laterally acting inhibitory activity in the developmental model. For the purpose of the computational model, we assume that B diffuses with a faster diffusion rate than A. Since cells produce these molecular species, only nodes of the lattice that contain cells produce morphogens.

Third, when cells encounter threshold levels of activator, they respond by producing a secreted, but otherwise immobile, molecular species to which cells attach. We term this substrate adhesion molecule (SAM) and identify it with fibronectin in the developmental model.³

Our simulation defines a “morphogenetic domain” on a square $n \times n$ lattice by an $n \times n$ matrix of 0's and 1's. A ‘0’ indicates a node outside of, and a ‘1’ indicates a node belonging to, the morphogenetic domain. The domain, all portions of which need not be connected, and which can have holes, can freely change at each time step and could be calculated by an auxiliary program. The only restriction on the domain is that it is a union of overlapping rectangles of at least two lattice points in height and width. In the current simulations, the morphogenetic domain is the entire $n \times n$ lattice. The components in the morphogenetic domain of the lattice include cells, activator molecules, inhibitor molecules, and SAM molecules. We store the concentration of each of these components as an $n \times n$ matrix of integers, where the matrix element (i,j) corresponds to the concentration of the various components at the node (i,j) .

Multiple cells and molecules of each type may occupy a node. Boundary conditions for the morphogenetic domain of the lattice are reflective (e.g., like the cushions of a pool table), so that particles (cells or molecules) cannot diffuse beyond the domain boundary. Diffusion of cells and molecules in directions crossing the boundary has zero probability while the sum of probabilities of diffusing in permitted directions and resting is equal to 1. If the morphogenetic domain contains two noncontiguous regions, then the various activities will occur in each region with no communication between them.

We initially distribute a fixed number of cells uniformly on a disc-shaped region centered in the morphogenetic domain of the lattice. We set initial densities of activator, inhibitor, and SAM to zero. The total number of cells remains constant throughout the simulation and cells secrete activator, inhibitor, and SAM molecules. Activator and inhibitor molecules diffuse through the morphogenetic do-

main of the lattice at every time-step, while SAM diffuses only during the time-step in which it is secreted. The diffusing molecules at each node independently move one unit up, down, left, right, or rest. The probability of moving in any permitted direction is equal, while the probability of resting p_R is an adjustable parameter with any value between 0 and 1. A higher probability of resting corresponds to a lower rate of migration, so we define the rate of diffusion as $1 - p_R$.

Cells initially secrete a small basal amount of activator, A. Since model cells are points, we may view secretion as occurring only at cell boundaries. Increased levels of activator stimulate secretion of activator and inhibitor. The increase in activator and inhibitor secretion is linear with respect to activator levels up to a plateau level of production for each morphogen. We assume that inhibitor decreases the effective activator concentration. Because inhibitors of TGF- β activity may act post-secretion (Smith, 1999), we assume that inhibitor levels decrease activator levels without requiring the presence of cells. For additional details of the mathematical model of activation and inhibition and of the dynamics of SAM production and deposition, see the Appendices.

Cells may have an extended response to activator levels since they continue to produce fibronectin for hours even after TGF- β is removed (Leonard et al., 1991). Thus, once threshold levels of activator appear at a node, we continue SAM production at that node for 5 h, independent of subsequent lower levels of activator. Keeping track of nodes that have seen threshold levels of activator is more computationally efficient than keeping track of the exposure of thousands of cells and is a good approximation since the diffusion of cells in our simulation is relatively slow.

Simulation results that depict cells represent SAM-attached cells as black pixels and unattached cells as gray pixels. This representation corresponds to the appearance of cells in micromass cultures visualized by Hoffman Modulation Contrast microscopy, where the rounded cells in condensations appear darker than the flatter cells outside the condensations.

For simplicity, the computational model we used in our initial study did not include assumption (vii) and the corresponding portion of assumption (v) of the developmental model. This omission facilitated calculation at the possible expense of detailed correspondence between *in silico* and *in vitro* results. The model, however, permits straightforward incorporation of a cell adhesion protein (and other similar cell properties and products) in subsequent studies.

Smoothing algorithm

Local inhomogeneity in the cell pattern results naturally from the discrete local rules of our CA. Smoothing produces a more realistic visual representation since it depicts cells as occupying the available culture plate surface, as in experiments, rather than as stacks. Although we assume the CA model starts with a “confluent” cell layer (every lattice

³ Because this study contains results both of *in vitro* and *in silico* experiments, we have chosen to use separate terms for the corresponding molecular entities in the two domains. In particular, we avoid using specific names of molecules for components of the computational model.

point occupied by a cell), randomly moving cells stack unevenly on nodes as they move along discrete channels (up, down, left, and right). This inhomogeneity is only a local artifact, however, and we can recover a confluent cell layer by averaging the cell distribution over a small neighborhood. In contrast, *in vitro*, confluent cells can slide past each other via tiny readjustments in their position, and the cultures exhibit no empty space between cells. We have therefore used a smoothing routine in visualizing cell distributions. Smoothing proceeded as follows: if more than one cell stacks on a node of the lattice, the displayed image averages the extra cell over the eight immediate neighbors of the node. Since our images are binary (a node is colored only if a cell is present), we define a density threshold of 0.5 cells per node for a cell to be visible.

Quantitative analysis

We compute the average peak interval for condensations in both cultures and simulations using the peak length method of Miura et al. (2000) for island patterns. We defined the peak length as the average distance between the center lines of chondrogenic areas. It measures the periodicity in the chondrogenic pattern and provides insight into the underlying mechanisms that form such patchy patterns (Miura et al., 2000). In particular, the average peak interval is independent of the width of the chondrogenic areas and the type of chondrogenic pattern (e.g., islands or stripes) (Miura et al., 2000). We used the algorithm described in Miura et al. (2000) to segregate chondrogenic and non-chondrogenic areas by binary image processing. After skeletonizing both the primary image and the inverted image and counting the number of peak and valley pixels, we used the program to measure the total lengths of peaks and valleys in the chondrogenic patterns. In certain cases, as

described in the text, we used a different quantitative measure of the chondrogenic pattern: the average island separation, defined as the average distance between each island center and the centers of its two closest neighbors. To represent the distribution of nearest neighbors, we measure the distance from the center of an island to the center of its nearest neighbor for all islands and count the fraction that fall in the range $\{0.8R, 1.2R\}$, where R is any real number. We plot this fraction as a function of R .

Results

Chemical peaks and cell clustering: standard “leg” conditions

In living leg cell cultures, the initial cell distribution is homogeneous, but, by the second day of growth, cells begin to form tightly packed focal condensations. Spacing between condensations is irregular, with a measurable average distance between centers (i.e., the average peak interval). The average condensation size generally increases in wing-cell cultures as the condensations expand and often merge (Downie and Newman, 1995; Leonard et al., 1991), whereas it stays fixed in leg-cell cultures where most condensations remain discrete (Downie and Newman, 1994, 1995). The terminal pattern in the leg cultures occurs around 3 days and in the wing cultures around 4 days. The condensations differentiate fully into cartilage nodules by day 6. Leg condensations visualized by Hoffman Contrast Modulation optics are evident at 48 h (Fig. 2a) and prominent after 72 h (Fig. 2b).

We measured the peak interval (see Materials and methods) and condensation “island” area in these cultures. For 13 leg cultures, the mean average peak interval was

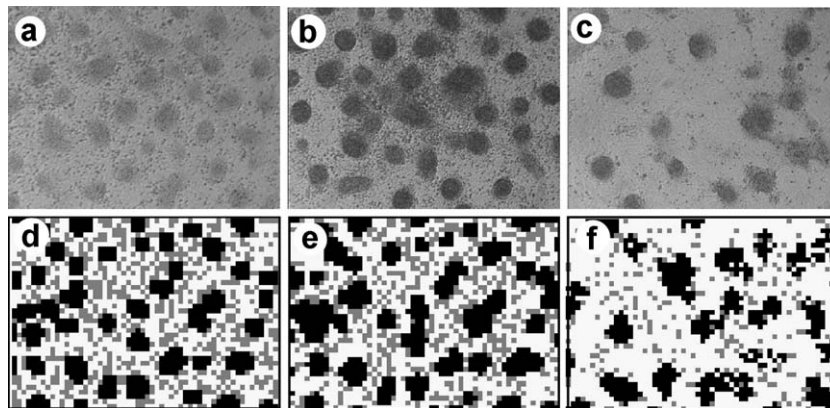


Fig. 2. Comparison of *in vitro* and *in silico* results for standard and diluted leg-cell cultures. Leg condensations visualized by Hoffman Contrast Modulation optics after (a) 48 h, (b) 72 h, and (c) for 15% dilution after 72 h. Actual size of each microscopic field (“high magnification view”) is 1×1.4 mm. Simulation results of smoothed free (gray) and stuck (black) cell locations after (a) 1000 time-steps for leg control parameters, (b) 4000 time-steps for leg control parameters, and (c) 4000 time-steps for 50% diluted leg-cell culture. Simulation parameters (“standard leg”) are diffusion rate of cells = 0.1, SAM production threshold = 1000, diffusion rate of A = 0.05, diffusion rate of B = 1, α_A = 0.09, α_B = 0.15, β_A = 1.1, A_{\max} = 55 and B_{\max} = 55. Simulation images correspond to high magnification views.

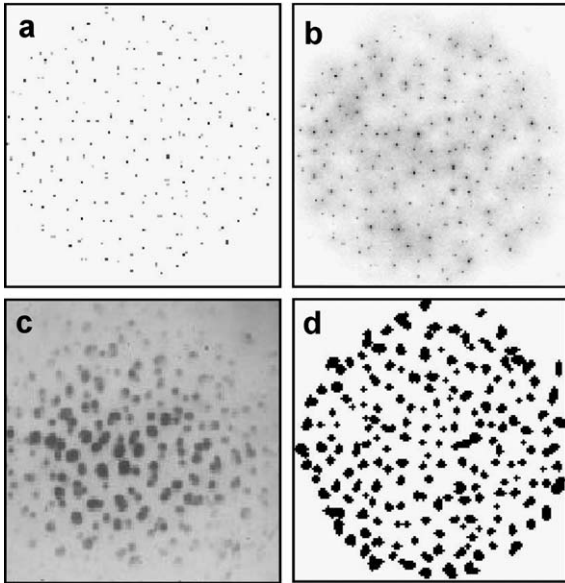


Fig. 3. Simulation results for scaled concentrations of key variables compared to the leg condensation pattern. (a) Morphogen A concentration, and (b) morphogen B concentration, after 4000 time-steps for control leg parameters; (c) leg condensations visualized by Hoffman Contrast Modulation optics after 72 h. Actual diameter of the circular culture is 3 mm (“low magnification view”); (d) scaled SAM density after 4000 time-steps for control leg parameters. Simulations correspond to low magnification views.

0.16 mm (range: 0.12–0.24 mm) and the mean average island area was 0.01 mm^2 (range: $0.005\text{--}0.028 \text{ mm}^2$).

We first explored the behavior of the CA model under conditions that simulate those of a typical limb-cell micro-mass culture. The initial micromass diameter *in vitro* is approximately 3 mm. Although living cells are plated at greater than confluent density in standard *in vitro* experiments (see e.g., Downie and Newman, 1995), a layer of ECM rapidly separates the cells, as in precondensed limb mesenchyme *in vivo* (Thorogood and Hinchliffe, 1975). Our simulations assumed a matrix to cell area ratio of 60:40, a

cell diameter of $15 \mu\text{m}$, and a “culture” spot diameter of 120 cells. Thus, we model cells with average density 1 on a disk 120 nodes in diameter (see Fig. 3).

As cells diffuse, one or more cells, or no cells, may occupy a node, so the production of activator and inhibitor varies over the lattice. Peaks of morphogen A and B begin to appear early in the simulation. Morphogen A peaks are only one or two nodes in size and levels drop from over 1000 units in a peak to zero units in immediately surrounding nodes (Fig. 3a). Morphogen B peaks are larger in size and much more diffuse (Fig. 3b). For comparison, we show *in vitro* condensations at the scale of a full micromass culture for the comparable experimental stage (Fig. 3c).

When the level of morphogen A in the simulation reaches a threshold, the cells begin to deposit SAM (Fig. 3d). Cells stick to these SAM deposits and local cell density increases. Activator, SAM, and cell concentration peaks are all co-local (compare Figs. 4d, e, and f).

Comparison of the development of condensations in experiments and simulations indicated that the period spanned by computational time-steps 1000–4000 corresponded to 50–72 h in culture. In particular, the cell density distribution after 1000 time-steps for the optimized parameters qualitatively resembles precartilaginous condensations after 50 h (compare Figs. 2a and d). During the next 3000 time-steps, the islands’ areas grow but their number remains unchanged, as in experiments after 72 h (compare Figs. 2a, b and d, e).

Simulated morphogen peaks, SAM deposits, and cell clusters develop in both time and space (Fig. 4). The number of SAM deposits does not increase between 1000 and 4000 time-steps (compare Figs. 4b and e), indicating that almost all activator peaks form within 1000 time-steps. Activator peaks remain co-local with SAM deposits. SAM clusters grow, however, and occasionally fuse over 4000 time-steps (compare Figs. 4b and e).

For our “standard leg” simulation parameters, which we found by trial and error, the average peak interval is 0.160

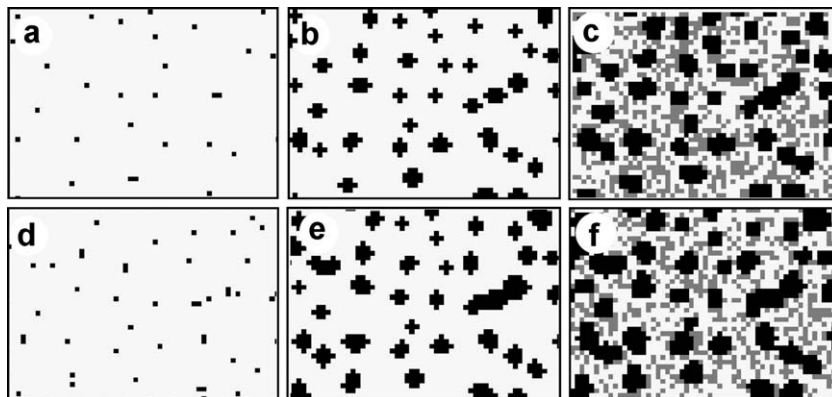


Fig. 4. Simulation dynamics of activator concentrations, SAM accumulation, and cell density over 1000–4000 time-steps for standard parameter vectors. (a) Morphogen A concentrations greater than threshold (1000 units), (b) SAM locations and (c) smoothed free (gray) and stuck (black) cell locations after 1000 time-steps. (d) Morphogen A concentrations greater than threshold (1000 units), (e) SAM locations, and (f) smoothed free (gray) and stuck (black) cell locations after 4000 time-steps. Simulation images correspond to high magnification view (see legend to Fig. 2).

Table 1

Sensitivity of average peak interval and island size to each key parameter when each parameter is varied independently near the standard point

Key parameter	Standard value and range varied	Sensitivity of average peak interval (mm)	Sensitivity of island size (mm ²)	Effect on average peak interval	Effect on island size
Upregulation of activator in response to activator	0.09 [0.075, 0.115]	−2.2	0.38	Decreases	Increases
Upregulation of inhibitor in response to activator	0.15 [0.12, 0.20]	1.4	−0.20	Increases	Decreases
Inhibition of activator in response to inhibitor	1.1 [1.02, 1.35]	0.3	−0.04	Increases	Decreases
Diffusion rate of activator	0.05 [0.015, 0.15]	0.64	1.0	Increases	Increases
Diffusion rate of inhibitor	1.0 [0.775, 1.00]	−0.36	0.04	Decreases	Increases
Cell dilution	0.0 [0.0, 0.70]	0.13	±0.01	Increases	Non-monotonic

mm (± 0.001 mm) and the average island size is 0.007 mm² (± 0.0004 mm²), which fall well within the experimental range. We needed to determine how our response variables (average peak interval and island size) depended on small changes in parameter values. The key parameters in the computational model are the diffusion rates of activator and inhibitor, the upregulation rates of activator and inhibitor in response to activator, the inhibitory effect of inhibitor on activator, and cell dilution. We sampled the “parameter space” defined by ranges of values of these key parameters around the standard values by measuring the effect of changing each key parameter independently (Table 1). We adjusted each key parameter independently since sampling the full multidimensional space in an exhaustive fashion was not feasible.

For each parameter, the sensitivity of each response variable (average peak interval and island size) is defined as the experimental range of the response variable divided by the extent of parameter variation for which simulation results remain within the experimental range. The sensitivity for a given parameter was either very small or there were clear monotonic trends as the parameter was varied. We did not adjust arbitrarily set parameters, such as the maximum per cell production of activator and inhibitor, the rate of cell diffusion, and the threshold level of activator that stimulates SAM production, in this set of simulations.

The trends summarized in Table 1 for parameters near the “standard leg” values provide insight into the mechanism of island formation in our computational model. Factors that directly or indirectly increase activator levels (upregulation of activator and diffusion of inhibitor) decrease the spacing between islands, and factors that directly or indirectly decrease activator levels (upregulation of inhibitor, inhibitor strength, diffusion of activator, and cell dilution) increase island spacing. In contrast, factors that increase the range of influence of an activator peak (upregulation of activator and activator diffusion) increase island size. Below, we investigate in more detail the quantitative effects of varying cell dilution and inhibitor strength in model simulations.

The range over which we may vary each parameter independently and the sets of antagonistic trends in Table 1 mean that many choices near our “standard leg”

parameter values will duplicate experimental patterns. For example, simulation trials with decreased diffusion rate of inhibitor and cell density diluted by 10% (Fig. 5, filled squares) also fall within the experimental range. For our model to provide a good representation of the in vitro system, small deviations from these “standard” parameter-space points should not greatly affect the response variables. As a test, we randomly chose parameter values within 5% of the standard values and found that the resulting patterns remained within the range of experimental measurements (Fig. 5). As expected from the trends in Table 1, there is an apparent inverse relationship between the average peak interval and the average island size in this regime.

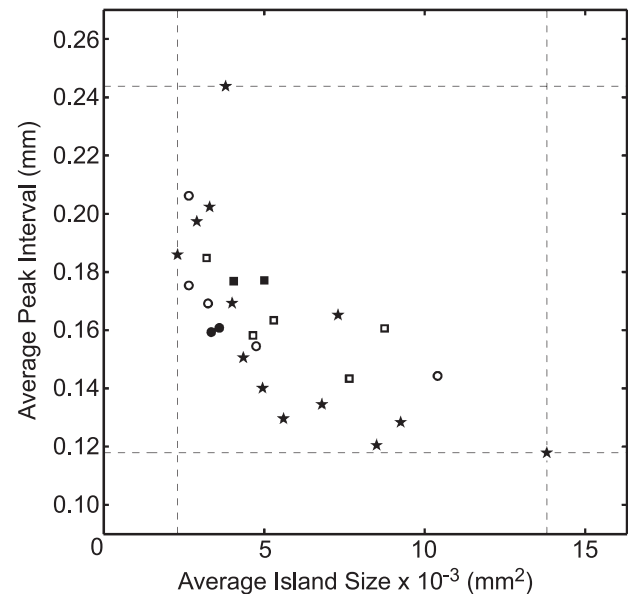


Fig. 5. Average peak interval vs. average island size for 13 experimental and 14 simulation points. For the 13 experiments (stars), the average peak interval ranges from 0.118 to 0.244 mm (horizontal dashed lines) and the average island size ranges from 0.0046 to 0.028 mm² (vertical dashed lines). Average peak interval vs. average island size for two simulation trials each of the “standard leg” (filled circles) and a nearby simulation point, “near standard leg” (filled squares), with cells diluted by 10% and the rate of diffusion of inhibitor decreased to 0.95. We also show average peak intervals vs. average island size for 10 simulations with parameters randomly chosen within 5% of the standard leg values (unfilled circles) and near the standard leg values (unfilled squares).

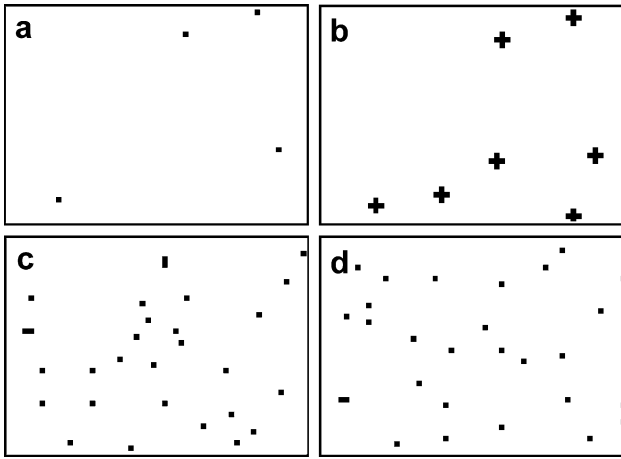


Fig. 6. Results of simulations without cell diffusion or without SAM. (a) Morphogen peaks greater than threshold (1000 units) and (b) SAM locations after 4000 time-steps with no cell diffusion. Morphogen peaks greater than threshold (1000 units) after (c) 1000 time-steps and (d) 4000 time-steps with no SAM production. Simulation images correspond to high magnification views.

Role of cell diffusion and SAM production

We compared the control simulation with simulations without cell diffusion or SAM production. Omitting cell diffusion greatly reduces the number of activator peaks formed within 4000 time-steps (compare Figs. 4d and 6a). Cell diffusion greatly facilitates the production of activator peaks. Also, without cell diffusion, SAM clusters do not grow (compare clusters from Fig. 6b with those of Fig. 4e), so, at least in this simple model, the growth of SAM islands requires cell diffusion. The need for diffusion may result

from the artificial constraint of constant cell area in our 2D representation; in culture, cells secrete ECM, which pushes them apart and into the third dimension (see Discussion). Without SAM production, morphogen peaks move (compare Figs. 4c and d), suggesting that these peaks require the formation of SAM islands to lock in place. In summary, cell diffusion along with activator-stimulated deposition of SAM causes cells to cluster, which creates islands of cells that are simultaneously sources of activator and inhibitor. Islands of cells maintain local elevated concentrations of activator even though the activator diffuses, effectively locking activator peaks in place.

Our computational implementation of the simple developmental model thus has the following features:

- (i) Interaction between cell-produced diffusible activating and inhibiting morphogens can create strong peaks in morphogen levels even when cells diffuse freely.
- (ii) Deposition of SAM occurs at sites of morphogen peaks and locks these peaks in place.
- (iii) Cells accumulate at SAM islands, giving rise to precartilaginous condensations.
- (iv) The number and position of precartilaginous condensations are determined early during the simulation, while condensation size increases with time.

Effect of cell dilution

Experimental manipulation of model parameters indicated a range for each key parameter that reproduced the standard leg pattern, defined by measurements of island size and average island spacing (Table 1; Fig. 5). We

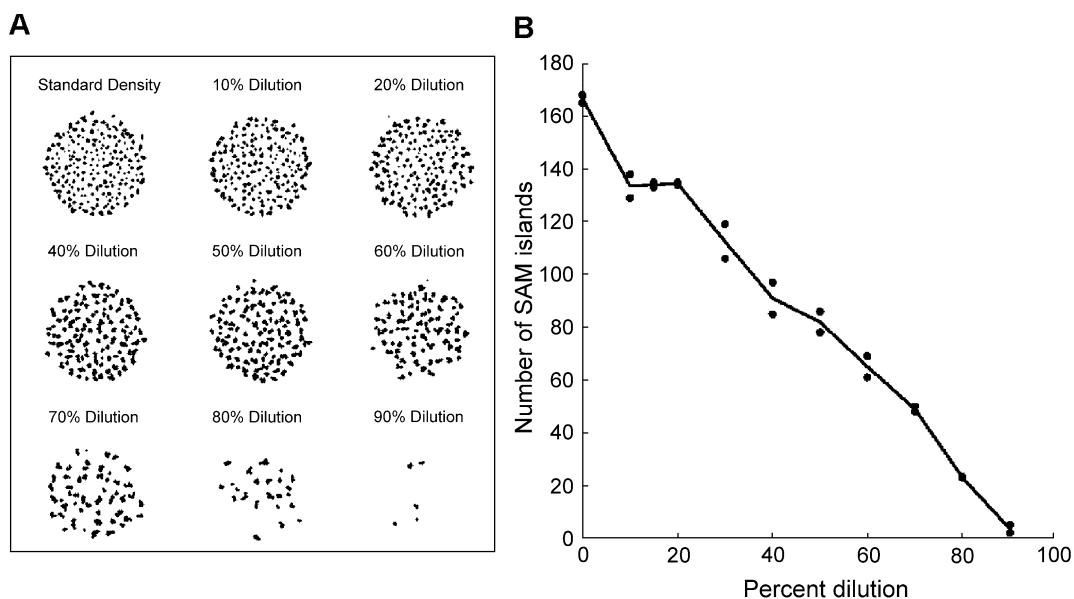


Fig. 7. Patterns for varying cell dilutions. (A) SAM island patterns and (B) number of SAM islands, for different cell dilutions after 4000 time-steps. In (B) we show results for two simulations with independent initial conditions. Simulation images correspond to low magnification view.

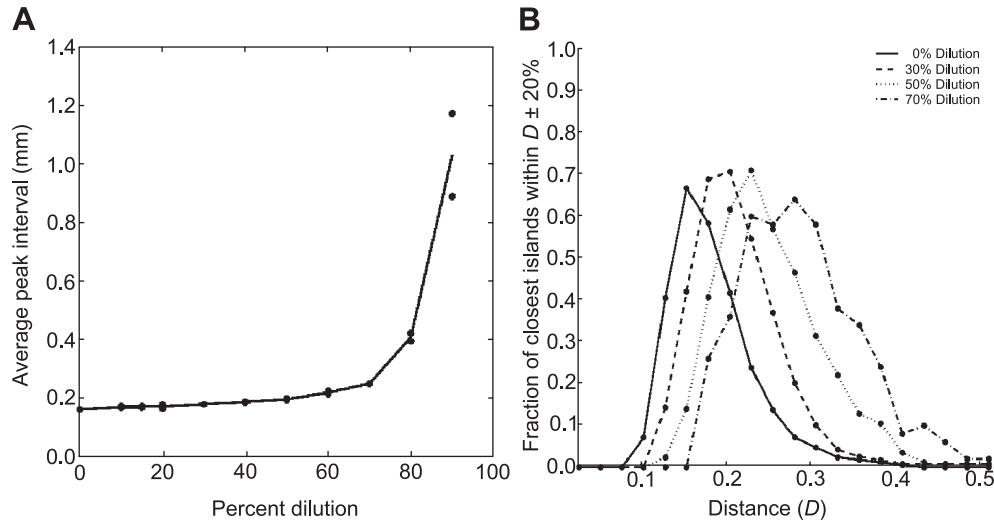


Fig. 8. Analysis of simulated chondrogenic patterns for varying cell dilutions. (A) Average peak interval in mm vs. percent dilution for two different simulations for each dilution value. (B) Fraction of islands with closest island found within a distance of $0.8 D$ to $1.2 D$ as a function of D (in mm) (see Materials and methods) for percent dilutions of 0% (solid line), 30% (dashed line), 50% (dotted line), and 70% (dash-dotted line).

next sought to determine whether experimental manipulation of the model parameters would reproduce altered patterns of condensation seen in *in vitro* experiments. For example, decreasing the initial cell density in *in vitro* experiments increased the average distance between condensations (Fig. 2c). Simulations with a smaller initial number of cells qualitatively reproduced these results (Fig. 2f). These 2D simulations required a higher dilution (50%) to match the appearance of cultures seeded at 85% of the control value (15% dilution). This disparity may relate to the nonlinear relation of plating efficiency to seeding density in the micromass cultures; that is, a 15% decrease in seeding density probably represented a greater than 15% reduction after the first day of culture.

We systematically analyzed how the simulation depended on cell density. The number of separate islands at 4000 time-steps decreased roughly linearly with the dilution percentage (Figs. 7A and B). The average peak interval (see Materials and methods) at 4000 time-steps was step-like in the dilution percentage, remaining between approximately 0.17 and 0.23 mm up to about 70% dilution, and rising sharply to about 0.9 mm between 80% and 90% dilution (Fig. 8A). We expect such behavior because the distance between islands of roughly constant size increases as the inverse of the number of islands. Significantly, and also expectedly, the greater the dilution, the broader the range of island spacings (Fig. 8B), that is, the spacing is less regular.

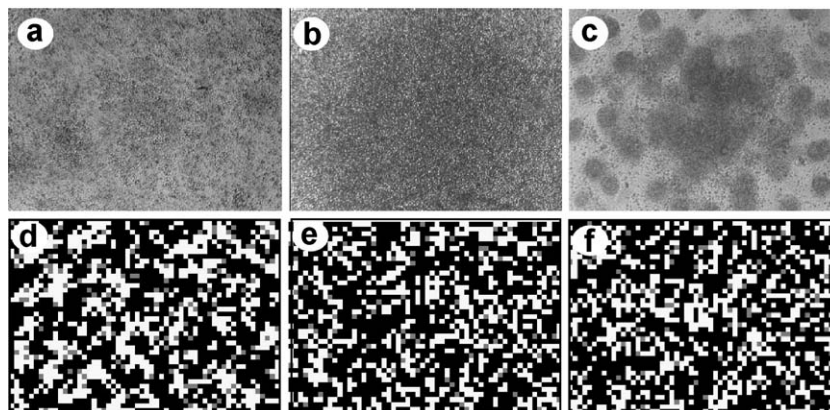


Fig. 9. Comparison of *in vitro* and *in silico* results for experimentally manipulated leg-cell cultures. Leg cultures (high magnification view) visualized by Hoffman Contrast Modulation optics after 72 h (a) transiently exposed to TGF- β on the day after plating, (b) with no FGF-induced lateral inhibition of condensation, and (c) transfected with capped mRNA specifying the NH₂-terminal domain of chicken fibronectin (see Materials and methods). Condensations have merged throughout the cultures in (a and b), and in the center of the culture in (c). Simulation results after 4000 time-steps of smoothed free (gray) and stuck (black) cell locations for (d) added activator, (e) no inhibitor, and (f) extra basal production of SAM. For added activator, we added 500 units of morphogen A to every node at 480 time-steps and removed it at 580 time-steps. For extra basal fibronectin production, 50% of cells produce an extra SAM molecule stochastically once every 2000 time-steps.

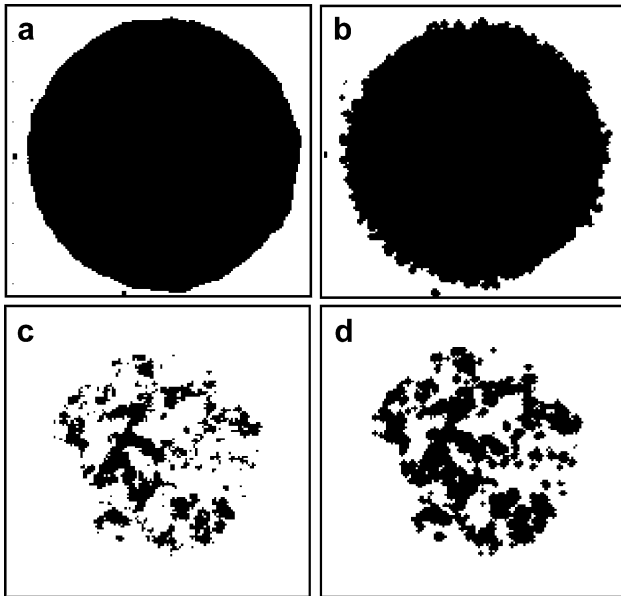


Fig. 10. Role of lateral inhibition in pattern formation in silico. Simulation results after 1000 time-steps for (a) morphogen A concentrations greater than threshold (1000 units) and (b) SAM locations for standard parameter values except with no production of inhibitor. Simulation results after 1000 time-steps for (c) morphogen A concentrations greater than threshold (1000 units) and (d) SAM locations, with no production of inhibitor with the following parameters: diffusion rate of cells = 0.1, SAM production threshold = 5000, diffusion rate of $A = 0.05$, diffusion rate of $B = 1$, $\alpha_A = 0.005$, $\alpha_B = 0$, $\beta_A = 0$, $A_{\max} = 5$, and $B_{\max} = 0$. The SAM pattern tracks the activator pattern even in the absence of inhibitor. Simulation images correspond to low magnification views (see legend to Fig. 3).

Stimulation by exogenous activator

In previous work, we studied the response of micro-mass cultures to exogenous TGF- β (Downie and Newman, 1994; Leonard et al., 1991). Transient (5–6 h) administration after one full day of culture was the most effective of a wide range of treatments in enhancing condensation and subsequent chondrogenesis (Leonard et al., 1991). Applying this protocol to leg cultures transformed the nodular morphology into a nearly continuous sheet, first of condensed cells, then cartilage (Downie and Newman, 1994) (Fig. 9a). In a corresponding simulation, we added 500 units of activator to every node of the culture after 480 time-steps (equivalent to 25 h) and removed it after 120 time-steps. After a total of 4000 time-steps, the simulation qualitatively reproduced the experimental results (Fig. 9d).

Role of lateral inhibitor

In a previous study (Moftah et al., 2002), we found that limb cells grown in the presence of serum formed discrete, nodular condensations as a result of a laterally acting inhibitor of condensation mediated by a fibroblast growth factor (FGF) receptor expressed at sites of incipient condensation. If we did not include ectoderm or ectodermally derived FGFs in leg-cell cultures, for example, a continuous sheet of condensed cells formed (see Fig. 9b) because of the lack of lateral inhibitor (Moftah et al., 2002). We therefore performed a simulation using standard “leg” parameters but eliminated the production of inhibitor. Within 1000 time-steps, SAM

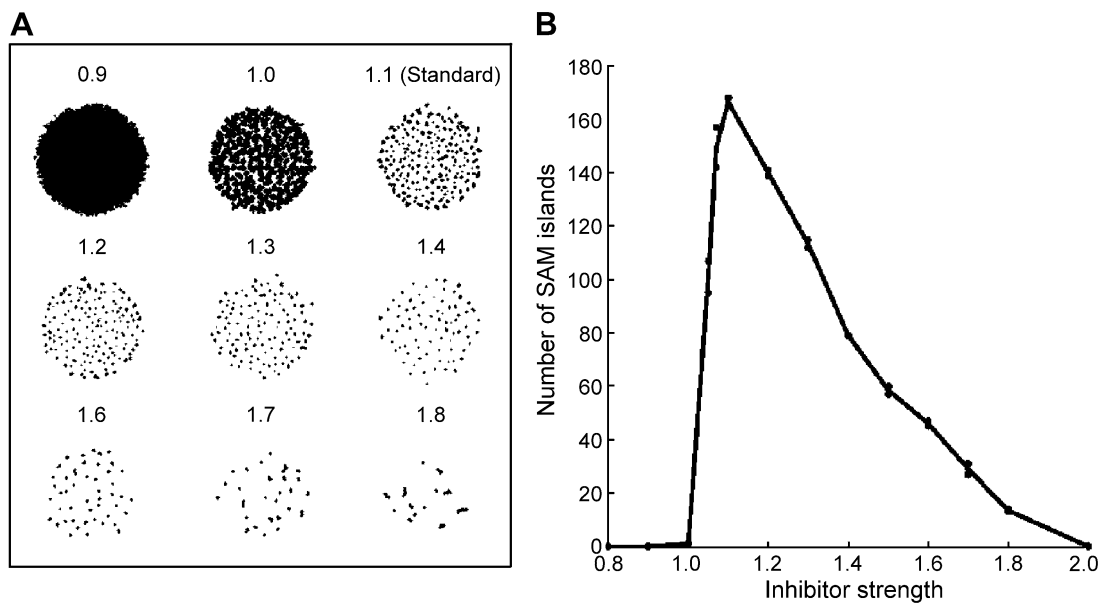


Fig. 11. Pattern formation for varying inhibitor strengths. (A) SAM island patterns; (B) number of SAM islands for different inhibitor strengths after 4000 time-steps. (B) shows two simulations with independent initial conditions for each inhibitor strength. Simulation images correspond to low magnification views.

covered the entire lattice occupied by cells, and cells formed broad, confluent patches (Fig. 9e). Figs. 10a and b show the distribution of activator and SAM after 1000 time-steps for simulations with no inhibitor. This set of parameters thus requires the inhibitor in order to generate the standard nodular pattern. Other parameter sets did not require the inhibitor to form distinct activator peaks (Fig. 10c). The SAM clusters that form under these conditions (Fig. 10d), however, differ in appearance from those of the control (compare Figs. 4b and 10d) since the peaks are not isolated, periodically spaced, or regular in size.

We analyzed systematically the pattern's dependence on the inhibitor. Varying the inhibitor strength β_A (the degree to which inhibitor suppresses activator; see Appendix A) between 0.9 and 1.8 led to SAM island patterns that ranged from entirely confluent (0.9) to focal with an apparently regular distribution (e.g., 1.1) to focal but apparently irregular (e.g., 1.7) (Fig. 11A). For β_A less than or equal to 1, activator levels dominate inhibitor levels during SAM deposition, and islands are confluent (Fig. 11A). For β_A above 1, the pattern undergoes an abrupt transition from a single island to many separate islands (Fig. 11B). This phenomenon resembles the “percolation transition” characteristic of a wide range of many-component physical systems with some random properties (Sahimi, 1994).

Island separation (see Materials and methods) is zero for both the fully confluent and interconnected islands, and is positive for inhibitor strengths above 1.0 (Fig. 12A). Fig. 12A also shows the average peak interval (see

Materials and methods) for various inhibitor strengths that produce disconnected islands. The distribution of island spacings tends to broaden with increasing inhibitor strength (above 1) (Fig. 12B). Large inhibitor strengths did not correlate with pattern regularity. Indeed, in the cases we examined, the narrowest distribution of island spacings was for $\beta_A = 1.3$ (Fig. 12B).

Constitutively expressed SAM

In another experiment, we transfected cells with capped mRNA encoding the NH₂-terminal heparin binding domain of fibronectin, a protein domain known to mediate condensation in limb bud mesenchyme (Downie and Newman, 1995; Frenz et al., 1989b). In these cultures, condensations tend to become confluent, particularly in central regions (Fig. 9c). In the corresponding simulation, 50% of the cells (randomly chosen; to correspond to typical transfection efficiency) produced an extra SAM unit at an average rate of once every 2000 time-steps, regardless of local activator concentration. After 4000 time-steps, simulated transfected cultures had many confluent condensations (Fig. 9f), qualitatively similar to the experiment.

We could not always distinguish experimental results for added TGF- β (Fig. 9a), low inhibitor (Fig. 9b), and transfected fibronectin NH₂-domain (Fig. 9c) from one another in *in vitro* experiments nor based on the developmental model (see above) would we expect to. In particular, in each of these cases, we expect, for different reasons, enlargement of the activated (condensing, chon-

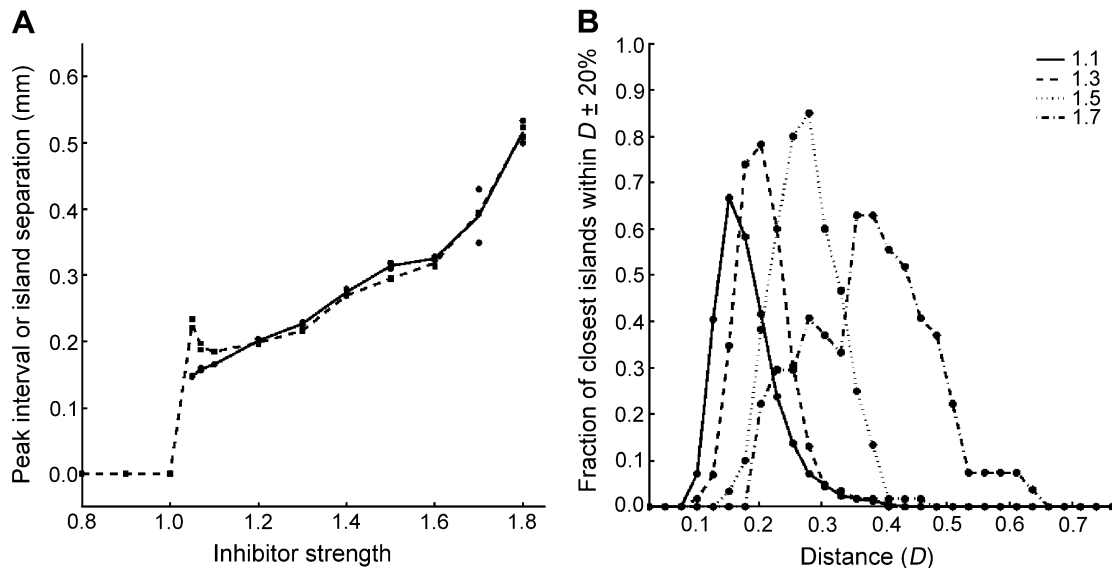


Fig. 12. Analysis of simulated SAM islands for varying inhibitor strengths. (A) Average peak interval (filled circles) and average island separation (filled squares) in mm vs. inhibitor strength for two different simulations for each inhibitor strength. We show the average peak interval alone for inhibitor strengths with disconnected SAM islands. The average island separation is 0 when the condensation islands are fully confluent or connected (inhibitor strength ≤ 1). (B) Fraction of islands with the closest island found within a distance between $0.8 D$ and $1.2 D$ as a function of D (in mm) (see Materials and methods) for inhibitor strength equal to 1.1 (solid line), 1.3 (dashed line), 1.5 (dotted line), and 1.7 (dash-dotted line).

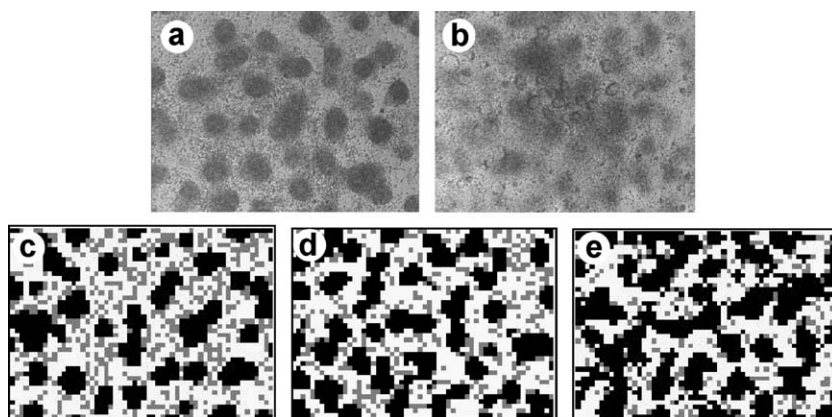


Fig. 13. Test of two hypotheses for the difference between leg and wing culture patterns. High magnification views visualized by Hoffman Contrast Modulation optics after 72 h of (a) leg-cell culture and (b) wing-cell culture. Simulation results after 4000 time-steps of smoothed free (gray) and stuck (black) cell locations for (c) control leg parameters, (d) SAM production decreased by a factor of 200, and (e) SAM production decreased by a factor of 200 and decreased activation of inhibitor α_B from 0.15 to 0.11.

drogenic) zones at the expense of the inhibited zones. The simulation results for the corresponding *in silico* manipulations (Figs. 9d–f) also generally resemble one another.

Differences between leg and wing

Since our model, with the standard “leg” cell parameter values, qualitatively reproduced *in silico* several standard *in vitro* experiments, we used it to determine what differences between embryonic chicken forelimb (i.e., wing bud) and hindlimb (e.g., leg bud) cells might cause their different *in vitro* condensation patterns (Downie and Newman, 1994, 1995). Condensations in wing-cell cultures (Fig. 13b) have a larger average island size after 72 h than in leg cultures (Figs. 2b and 13a) and eventually become confluent (Leonard et al., 1991).

Wing cells produce less fibronectin as a proportion of total protein than leg cells and produce a smaller incremental amount of fibronectin relative to basal levels under TGF- β stimulation (Downie and Newman, 1995). We tested whether this difference alone could account for the pattern differences by decreasing SAM production by a factor of 200. In these simulations, islands remained discrete and their size decreased slightly (Fig. 13d), contrary to the observed wing-cell pattern (Fig. 13b).

In addition to producing less fibronectin, wing cells might produce less additional inhibitor in response to equivalent amounts of activator (TGF- β) (Newman, 1996). Indeed, wing and leg cells differ in their expression of the genes encoding transcription factors Txb4 and Txb5 (Takeuchi et al., 1999), which regulate expression of FGFs (Takeuchi et al., 2003). FGF expression, in turn, relates to the production of a perinodular inhibitor of condensation in the developing limb (Moftah et al., 2002). We therefore performed simulations that both kept

the SAM production rate low relative to the standard leg conditions and also decreased the activation of inhibitor from 0.15 to 0.11. In this case, islands were broader and less discrete (Fig. 13e), corresponding better to the experimental wing pattern.

Discussion

Our computational model contains an activator–inhibitor circuit that corresponds to a reaction–diffusion process. It also includes a set of rules that permits model cells to interact with the SAM they, and nearby cells, deposit. The sophistication of the rules therefore makes this biological “lattice-gas” cellular automaton (Alber et al., 2004; Wolf-Gladrow, 2000) a hybrid between classic CA (e.g., Wolfram, 2002) and differential-equation-based approaches (e.g., Painter et al., 2000), and allows us to assess independently the roles of reaction–diffusion patterning and cell–substrate adhesion in generating patterns of precartilage condensation.

For example, we showed that omitting inhibition made the simulation (Fig. 9d) less similar to experimental leg cultures (Fig. 2b) than the simulation that included inhibitor (Fig. 2d). Although for some choices of parameters island-type patterns formed without inhibitor (Fig. 10d), these patterns exhibited no evident regular spacing between islands. While these simulations show that cell–aggregation-based patterning can clearly occur with cell–substrate adhesion in the absence of inhibition (see also Zeng et al., 2003), theoretical arguments suggest that biological structures that require reliable regular patterns are likely to employ an inhibitory effect that originates from the centers of activation and restricts the lateral spread of the activator’s effect (Boissonade et al., 1994; Meinhardt and Gierer, 2000; Turing, 1952). Our “standard model” contains such a lateral inhibitor. Experi-

tal findings in the limb also indicate the existence of lateral inhibition of chondrogenesis (Hurlle et al., 1989; Mofteh et al., 2002).

Once we determined the standard conditions for simulating leg culture patterns, systematic variation of the parameters provided insight into the origins of pattern regularity (Table 1; Fig. 5). For example, the regularity of the SAM island distribution broke down when the cells were too dilute (Figs. 7 and 8) or when the range of inhibitor activity was too short (Figs. 11 and 12). Such results suggest how alterations of developmental parameters may create morphological novelty during development and evolution (Salazar-Ciudad et al., 2003).

We note that dynamical models based on different sets of assumptions from those used here, for example, direct cell–cell contact (Edelstein-Keshet and Ermentrout, 1990a,b) or cell traction (Murray and Oster, 1984; Ngwa and Maini, 1995), are capable of giving rise to patterns of cell association analogous to mesenchymal condensations. Experimental evidence on limb bud mesenchyme in vitro and developing limbs in vivo, however, supports the idea that the pattern of precartilaginous condensations arises in response to a chemical prepattern rather than directly through biomechanical effects (reviewed in Newman and Tomasek, 1996).

Miura and Shiota (2000b) were unable to conclude whether a cell-sorting mechanism using differential adhesion, but not lateral inhibition, could account for the periodicity of condensations (see also Zeng et al., 2003). Subsequent work indicated that such inhibitory effects are indeed present in vitro and in vivo, where they are subject to modulation by FGFs (Mofteh et al., 2002). Our simulations indicate that attenuation of inhibitor reduces periodicity in the condensation pattern, leading to results that resemble chicken wing-cell cultures (Fig. 13b) and mouse limb-cell cultures (Miura and Shiota, 2000b), more than chicken leg-cell cultures (Figs. 2b and 13a). These results did not employ assumption (vii) of our developmental model, that is, direct cell–cell adhesion by CAMs, such as N-cadherin. We are currently testing whether this mechanism can contribute to the regularity of the condensation pattern despite attenuated lateral inhibition.

Our success in obtaining a non-trivial parameter set that reproduced the number, size, and distribution of condensations of the standard culture, and the ability of this parameter set to produce qualitatively accurate simulations of cultures under diluted, TGF- β -stimulated, reduced-inhibitor, and fibronectin-transfected conditions, gives us confidence that our CA model captures important aspects of development. Because we could simulate differences between wing- and leg-cell in vitro condensation patterns by altering constitutive properties of cells that plausibly relate to differences in expression of transcription factors such as Tbx4 and Tbx5, the model has predictive power for multiple cell types.

One unresolved issue is the lack of good correspondence in the timing of the initial steps of in vitro and its in silico condensation. A pattern corresponding to a 48-h culture takes about 1000 time-steps, and a stationary pattern, corresponding to about 72 h in vitro, takes another 3000 time-steps. Since the processes involved in the simulation are essentially uniform, the disparity is most likely due to a lag in the culture's recovery from cell dissociation, or possibly a developmentally regulated delay in the morphogenetic response of cells during patterning (Newman and Frisch, 1979; Toole et al., 1972). The lack of cell–cell adhesion may also play a role.

Such examples, in which comparison of simulation with experiment suggests missing elements in the model, highlight the power of this approach in framing experimental hypotheses. Indeed, CA modeling as presented here, far from being a retrospective summary of existing experiments, is actually a parallel means of experimentation on systems, such as chondrogenic patterning in vitro, with partially characterized relevant variables and parameters. It is an efficient and cost-effective tool for homing in on the range of potential manipulations that can provide decisive tests of in vitro and in vivo experimental models.

The specific model described here, with changes in geometry and parameter choices, should apply to other quasi-2D situations, such as epithelial pigment patterns (Kondo and Asai, 1995) and feather bud formation (Jiang et al., 1999; Prum and Williamson, 2002). Fully three-dimensional developmental problems, such as skeletal patterning during vertebrate limb development, will likely require more elaborate cell automata-based strategies such as those based on the extended Potts model (Glazier and Graner, 1993; Izaguirre et al., 2004; Marée and Hogeweg, 2001) in conjunction with continuum approaches (Dillon et al., 2003; Hentschel et al., in press).

Acknowledgments

We thank Ms. Sovannary Tan for technical assistance. We acknowledge grant support from the National Science Foundation (IBN-0083653, under the Biocomplexity Initiative, to M.A., J.A.G. and S.A.N., and IBN-0090499 to S.A.N.). We also acknowledge support for G.L.T. from CAPES-Brazil, for J.A.G. from NASA (NAG 2-1619), and for M.K. from the Notre Dame Center for the Study of Biocomplexity and Center for Applied Mathematics.

Appendix A. Mathematical model for activation and inhibition

We model activation and inhibition at each node as follows: let C_A and C_B be the concentrations of morph-

ogens A and B, respectively. Let n_c be the number of cells at the node. For low levels of morphogen A, morphogen A activates itself in proportion to some parameter $\alpha_A (>0)$ and to the number of cells:

$$C_A = C_A + (\alpha_A C_A) n_c. \quad (1)$$

For high levels of morphogen A, however, each cell can only produce a maximum level A_{\max} of activator:

$$C_A = C_A + \min(\alpha_A C_A, A_{\max}) n_c. \quad (2)$$

We can express this dependence with a step-function Φ_A :

$$C_A = C_A + \Phi_A(n_c), \quad (3)$$

where

$$\Phi_A(n_c) = \{(\alpha_A C_A) n_c \text{ if } (\alpha_A C_A) n_c < A_{\max}, \text{ otherwise } A_{\max} n_c\}. \quad (4)$$

Low levels of morphogen A activate morphogen B in proportion to a parameter $\alpha_B (>0)$ and to the number of cells:

$$C_B = C_B + (\alpha_B C_A) n_c. \quad (5)$$

For high levels of morphogen A, however, each cell can only produce a maximum level B_{\max} of activator:

$$C_B = C_B + \min(\alpha_B C_A, B_{\max}) n_c. \quad (6)$$

We can express this dependence with a step-function Φ_B :

$$C_B = C_B + \Phi_B(n_c), \quad (7)$$

where

$$\Phi_B(n_c) = \{(\alpha_B C_A) \text{ if } (\alpha_B C_A) n_c < B_{\max}, \text{ otherwise } B_{\max} n_c\}. \quad (8)$$

Morphogen B inhibits morphogen A in proportion to a parameter $\beta_A (>0)$ (the strength of inhibition) throughout the lattice, independent of the concentration of cells:

$$C_A = \max(C_A - \beta_A C_B, 0). \quad (9)$$

Also, morphogen B decays as it inhibits morphogen A:

$$C_B = C_B - \Delta C_A / \beta_A, \quad (10)$$

where ΔC_A is the change due to inhibition.

The net activation and inhibition are:

$$\begin{aligned} \delta C_A / \delta t &= \Phi_A(n_c) - \beta_A C_B, \\ \delta C_B / \delta t &= \Phi_B(n_c) - \Delta C_A / \beta_A. \end{aligned} \quad (11)$$

Appendix B. Dynamics of SAM production and deposition

After we update the morphogen concentrations, if the concentration of morphogen A exceeds a threshold A_t at a node, each cell at that node creates a SAM “molecule” (i.e., a collection of molecules that act as a unit) with probability p_f . SAM randomly diffuses for a distance of only one node, after which it no longer diffuses. The single diffusion step allows the SAM to reach neighboring nodes, so that the SAM deposits may extend to and affect the immediate neighborhood of a cell. As the number of SAM molecules in the extracellular matrix increases, the rate of random cell movement (“cell diffusion”) decreases. However, the number of cells that may become trapped within a small unit area has an upper limit. Our model allows up to f SAM molecules per node and specifies that up to n_f cells can attach to each SAM molecule. In the in vitro system, the amount of fibronectin that may reside at any site is limited, and some is always lost to the medium. Therefore, if a SAM molecule diffuses to a node that has excess SAM molecules, we delete it. Cells coexisting at a node with SAM molecules stick to each available SAM molecule at a rate p_s and unstick at a rate $(1 - p_s)$. Since all cells are equivalent, we model attachment in the following way: at each time step, we assume that all cells are initially unattached to SAM. Then, each cell has a probability p_s of sticking to each available SAM molecule. Once a SAM molecule has n_f attached cells, it can no longer bind cells during that time-step. Since a node can hold only f SAM molecules and only n_f cells may attach to each SAM molecule, the maximum number of cells stuck at each node is fn_f .

References

- Alber, M.S., Jiang, Y., Kiskowski, M.A., 2004. Lattice gas cellular automation model for rippling and aggregation in myxobacteria. *Physica D* 191, 343–358.
- Boissonade, J., Dulos, E., DeKepper, P., 1994. Turing patterns: from myth to reality. In: Kapral, R., Showalter, K. (Eds.), *Chemical Waves and Patterns*. Kluwer Academic Publishing, Boston, pp. 221–268.
- Brand, B., Christ, B., Jacob, H.J., 1985. An experimental analysis of the developmental capacities of distal parts of avian leg buds. *Am. J. Anat.* 173, 321–340.
- Chimal-Monroy, J., Rodriguez-Leon, J., Montero, J.A., Ganán, Y., Macías, D., Merino, R., Hurle, J.M., 2003. Analysis of the molecular cascade responsible for mesodermal limb chondrogenesis: sox genes and BMP signaling. *Dev. Biol.* 257, 292–301.
- Delise, A.M., Tuan, R.S., 2002. Analysis of N-cadherin function in limb mesenchymal chondrogenesis in vitro. *Dev. Dyn.* 225, 195–204.
- Delise, A.M., Stringa, E., Woodward, W.A., Mello, M.A., Tuan, R.S., 2000. Embryonic limb mesenchyme micromass culture as an in vitro model for chondrogenesis and cartilage maturation. *Methods Mol. Biol.* 137, 359–375.
- Dewdney, A.K., 1987. The game of life acquires some successors in three dimensions. *Sci. Am.* 224, 112–118.
- Dillon, R., Gadgil, C., Othmer, H.G., 2003. Short- and long-range effects of

- Sonic hedgehog in limb development. *Proc. Natl. Acad. Sci. U. S. A.* 100, 10152–10157.
- Downie, S.A., Newman, S.A., 1994. Morphogenetic differences between fore and hind limb precartilaginous mesenchyme: relation to mechanisms of skeletal pattern formation. *Dev. Biol.* 162, 195–208.
- Downie, S.A., Newman, S.A., 1995. Different roles for fibronectin in the generation of fore and hind limb precartilaginous condensations. *Dev. Biol.* 172, 519–530.
- Edelstein-Keshet, L., Ermentrout, G.B., 1990a. Contact response of cells can mediate morphogenetic pattern formation. *Differentiation* 45, 147–159.
- Edelstein-Keshet, L., Ermentrout, G.B., 1990b. Models for contact-mediated pattern formation: cells that form parallel arrays. *J. Math. Biol.* 29, 33–58.
- Ermentrout, G.B., Edelstein-Keshet, L., 1993. Cellular automata approaches to biological modeling. *J. Theor. Biol.* 160, 97–133.
- Frenz, D.A., Akiyama, S.K., Paulsen, D.F., Newman, S.A., 1989a. Latex beads as probes of cell surface–extracellular matrix interactions during chondrogenesis: evidence for a role for amino-terminal heparin-binding domain of fibronectin. *Dev. Biol.* 136, 87–96.
- Frenz, D.A., Jaikaria, N.S., Newman, S.A., 1989b. The mechanism of precartilaginous mesenchymal condensation: a major role for interaction of the cell surface with the amino-terminal heparin-binding domain of fibronectin. *Dev. Biol.* 136, 97–103.
- Glazier, J.A., Graner, F., 1993. A simulation of the differential adhesion driven rearrangement of biological cells. *Phys. Rev., E* 47, 2128–2154.
- Hall, B.K., Miyake, T., 1995. Divide, accumulate, differentiate: cell condensation in skeletal development revisited. *Int. J. Dev. Biol.* 39, 881–893.
- Hall, B.K., Miyake, T., 2000. All for one and one for all: condensations and the initiation of skeletal development. *BioEssays* 22, 138–147.
- Hamburger, V., Hamilton, H.L., 1951. A series of normal stages in the development of the chick embryo. *J. Morphol.* 88, 49–92.
- Hentschel, H.G.E., Glimm, T., Glazier, J.A., Newman, S.A., 2004. Dynamical mechanisms for skeletal pattern formation in the vertebrate limb. *Proc. Roy. Soc. Lond. Ser. B* (in press).
- Hurle, J.M., Gañan, Y., Macias, D., 1989. Experimental analysis of the in vivo chondrogenic potential of the interdigital mesenchyme of the chick leg bud subjected to local ectodermal removal. *Dev. Biol.* 132, 368–374.
- Izaguirre, J.A., Chaturvedi, R., Huang, C., Cickovski, T., Thomas, G., Forgacs, G., Alber, M., Hentschel, G., Newman, S.A., Glazier, J.A., 2004. COMPUCELL, a multi-model framework for simulation of morphogenesis. *Bioinformatics* 20, 1129–1137.
- Jiang, T., Jung, H., Widelitz, R.B., Chuong, C., 1999. Self-organization of periodic patterns by dissociated feather mesenchymal cells and the regulation of size, number and spacing of primordia. *Development* 126, 4997–5009.
- Kaplan, D.T., Smith, J.M., Saxberg, B.E., Cohen, R.J., 1988. Nonlinear dynamics in cardiac conduction. *Math. Biosci.* 90, 19–48.
- Kreft, J.U., Picioreanu, C., Wimpenny, J.W., van Loosdrecht, M.C., 2001. Individual-based modelling of biofilms. *Microbiology* 147, 2897–2912.
- Kondo, S., Asai, R., 1995. A reaction–diffusion wave on the skin of the marine angelfish *Pomacanthus*. *Nature* 376, 765–768.
- Leonard, C.M., Fuld, H., Frenz, D.A., Downie, S.A., Massagué, J., Newman, S.A., 1991. Role of transforming growth factor-beta in chondrogenic pattern formation in the embryonic limb: stimulation of mesenchymal condensation and fibronectin gene expression by exogenous TGF-beta-like activity. *Dev. Biol.* 145, 99–109.
- Marée, A.F., Hogeweg, P., 2001. How amoeboids self-organize into a fruiting body: multicellular coordination in *Dictyostelium discoideum*. *Proc. Natl. Acad. Sci. U. S. A.* 98, 3879–3883.
- Meinhardt, H., Gierer, A., 2000. Pattern formation by local self-activation and lateral inhibition. *BioEssays* 22, 753–760.
- Merino, R., Gañan, Y., Macias, D., Economides, A.N., Sampath, K.T., Hurle, J.M., 1998. Morphogenesis of digits in the avian limb is controlled by FGFs, TGFbetas, and noggin through BMP signaling. *Dev. Biol.* 200, 35–45.
- Miura, T., Shiota, K., 2000a. TGFbeta2 acts as an “activator” molecule in reaction–diffusion model and is involved in cell sorting phenomenon in mouse limb micromass culture. *Dev. Dyn.* 217, 241–249.
- Miura, T., Shiota, K., 2000b. Extracellular matrix environment influences chondrogenic pattern formation in limb bud micromass culture: experimental verification of theoretical models. *Anat. Rec.* 258, 100–107.
- Miura, T., Komori, M., Shiota, K., 2000. A novel method for analysis of the periodicity of chondrogenic patterns in limb bud cell culture: correlation of in vitro pattern formation with theoretical models. *Anat. Embryol. (Berlin)* 201, 419–428.
- Moftah, M.Z., Downie, S.A., Bronstein, N.B., Mezentseva, N., Pu, J., Maher, P.A., Newman, S.A., 2002. Ectodermal FGFs induce perinodular inhibition of limb chondrogenesis in vitro and in vivo via FGF receptor 2. *Dev. Biol.* 249, 270–282.
- Murray, J.D., Oster, G.F., 1984. Cell traction models for generating pattern and form in morphogenesis. *J. Math. Biol.* 19, 265–279.
- Newman, S.A., 1977. Lineage and pattern in the developing wing bud. In: Ede, D.A., Hinchliffe, J.R., Balls, M. (Eds.), *Vertebrate Limb and Somite Morphogenesis*. Cambridge Univ. Press, Cambridge, pp. 181–197.
- Newman, S.A., 1988. Lineage and pattern in the developing vertebrate limb. *Trends Genet.* 4, 329–332.
- Newman, S.A., 1996. Sticky fingers: Hox genes and cell adhesion in vertebrate development. *BioEssays* 20, 662–668.
- Newman, S.A., Frisch, H.L., 1979. Dynamics of skeletal pattern formation in developing chick limb. *Science* 205, 662–668.
- Newman, S.A., Tomasek, J.J., 1996. Morphogenesis of connective tissues. In: Comper, W.D. (Ed.), *Extracellular Matrix Molecular Components and Interactions*, vol. 2. Harwood Academic Publishers, Amsterdam, pp. 335–369.
- Newman, S.A., Pautou, M.-P., Kieny, M., 1981. The distal boundary of myogenic primordia in chimeric avian limb buds and its relation to an accessible population of cartilage progenitor cells. *Dev. Biol.* 84, 440–448.
- Ngwa, G.A., Maini, P.K., 1995. Spatio-temporal patterns in a mechanical model for mesenchymal morphogenesis. *J. Math. Biol.* 33, 489–520.
- Oberlander, S.A., Tuan, R.S., 1994. Expression and functional involvement of N-cadherin in embryonic limb chondrogenesis. *Development* 120, 177–187.
- Painter, K.J., Maini, P.K., Othmer, H.G., 2000. Development and applications of a model for cellular response to multiple chemotactic cues. *J. Math. Biol.* 41, 285–314.
- Paulsen, D.F., Solursh, M., 1988. Microtiter micromass cultures of limb-bud mesenchymal cells. *In Vitro Cell Dev. Biol.* 24, 138–147.
- Prum, R.O., Williamson, S., 2002. Reaction–diffusion models of within-feather pigmentation patterning. *Proc. R. Soc. London, Ser. B Biol. Sci.* 269, 781–792.
- Pu, J., 1999. Studies of fibronectin regulation and expression during limb chondrogenesis. Ph.D. dissertation. Department of Cell Biology and Anatomy. New York Medical College, Valhalla, NY.
- Ros, M.A., Lyons, G.E., Mackem, S., Fallon, J.F., 1994. Recombinant limbs as a model to study homeobox gene regulation during limb development. *Dev. Biol.* 166, 59–72.
- Sahimi, M., 1994. *Applications of Percolation Theory*. Taylor & Francis, London.
- Salazar-Ciudad, I., Jernvall, J., Newman, S.A., 2003. Mechanisms of pattern formation in development and evolution. *Development* 130, 2027–2037.
- Smith, W.C., 1999. TGF beta inhibitors. New and unexpected requirements in vertebrate development. *Trends Genet.* 15, 3–5.
- Takeuchi, J.K., Koshihara-Takeuchi, K., Matsumoto, K., Vogel-Hopker, A., Naitoh-Matsuo, M., Ogura, K., Takahashi, N., Yasuda, K., Ogura, T., 1999. Tbx5 and Tbx4 genes determine the wing/leg identity of limb buds. *Nature* 398, 810–814.

- Takeuchi, J.K., Koshiba-Takeuchi, K., Suzuki, T., Kamimura, M., Ogura, K., Ogura, T., 2003. Tbx5 and Tbx4 trigger limb initiation through activation of the Wnt/Fgf signaling cascade. *Development* 130, 2729–2739.
- Tickle, C., 2003. Patterning systems—From one end of the limb to the other. *Dev. Cell* 4, 449–458.
- Toole, B.P., Jackson, G., Gross, J., 1972. Hyaluronate in morphogenesis: inhibition of chondrogenesis in vitro. *Proc. Natl. Acad. Sci. U. S. A.* 69, 1384–1386.
- Tsonis, P.A., Del Rio-Tsonis, K., Millan, J.L., Wheelock, M.J., 1994. Expression of N-cadherin and alkaline phosphatase in chick limb bud mesenchymal cells: regulation by 1,25-dihydroxyvitamin D3 or TGF-beta 1. *Exp. Cell Res.* 213, 433–437.
- Turing, A., 1952. The chemical basis of morphogenesis. *Philos. Trans. R. Soc. London, Ser. B* 237, 37–72.
- Widelitz, R.B., Jiang, T.X., Murray, B.A., Chuong, C.M., 1993. Adhesion molecules in skeletogenesis: II. Neural cell adhesion molecules mediate precartilaginous mesenchymal condensations and enhance chondrogenesis. *J. Cell. Physiol.* 156, 399–411.
- Winfree, A.T., Winfree, E.M., Seifert, H., 1985. Organizing centers in cellular excitable media. *Physica* 17D, 109–115.
- Wolf-Gladrow, D.A., 2000. *Lattice-Gas Cellular Automata and Lattice Boltzmann Models Lecture Notes in Mathematics*, vol. 1795. Springer, Berlin.
- Wolfram, S., 1983. Statistical mechanics of cellular automata. *Rev. Mod. Phys.* 55, 601–644.
- Wolfram, S., 1994a. Statistical mechanics of cellular automata. *Rev. Mod. Phys.* 55, 601–644.
- Wolfram, S., 1994b. *Cellular Automata and Complexity* Addison-Wesley, Reading.
- Wolfram, S., 2002. *A New Kind of Science*. Wolfram Media, Champaign, IL.
- Zeng, W., Thomas, G.L., Newman, S.A., Glazier, J.A., 2003. A novel mechanism for mesenchymal condensation during limb chondrogenesis in vitro. In: Capasso, V. (Ed.), *Mathematical Modeling and Computing in Biology and Medicine*, 5th ESMTB Conference 2002. Società Editrice Esculapio, Bologna, Italy, pp. 80–86.
- Zwilling, E., 1964. Development of fragmented and of dissociated limb bud mesoderm. *Dev. Biol.* 89, 20–37.